Laser ablation molecular isotopic spectroscopy: a novel tool to characterise the distribution of ^{13}C and ^{12}C on graphite after $^{13}CH_4$ tracer injection in Wendelstein 7-X

E. Wüst[a], T. Dittmar[a], C.Kawan[a], J. Romazanov[a], S. Brezinsek[a]
and the W7-X team[b]
[a]Forschungszentrum Jülich, Institut für Energie- und Klimaforschung
Plasmaphysik, 52425 Jülich, Germany
[b]T. Klinger et al, Nuclear Fusion 59 (2019) 112004

August 2, 2022

1 Introduction

Effects of plasma-wall interaction such as erosion of and deposition on Plasma-Facing Components (PFCs) are important for questions of material life time, operational regime and safety of fusion devices. In purely toroidal symmetry, as is present in tokamaks, several studies have been conducted to investigate all of thos aspects [12]. The aim for continuous operation of stellarators in complex 3D geometry make new studies in such devices necessary. Mayer et al. [10] observed the erosion and deposition patterns in Wendelstein 7-X (W7-X) with marker layers embedded in PFCs. Codes like ERO2.0 [13] are being developed to simulate plasma-wall interaction in fusion devices. Additional studies of carbon migration leading to deposition in stellarators are needed to test the codes in question and give valuable input for their further development [4].
Experiments in Operation Phase (OP) 1.2b of W7-X had been conducted for this reason, in which ^{13}C isotopically marked methane was injected into a hydrogen plasma [4]. The distribution of deposited ^{13}C on PFCs part of the non-actively cooled fine grain graphite Test Divertor Unit (TDU) are now analysed in post-mortem studies with the components removed from the machine. Methods like Nuclear Reaction Analysis (NRA) or Secondary Ion Mass Spectroscopy (SIMS) are established techniques that have been used for deposition and erosion analyses using marker layers or injecting marker isotopes into the plasma [11] [8]. However, Divertor Units are currently completely exchanged for actively water cooled elements to be used in the upcoming OP of W7-X [2] [3]. The structure supplying the coolant to the divertor units will make removal for post-mortem analyses more challenging. Accordingly, the development of a method for carbon isotope distinction that can be used in-situ without removal of PFCs is of interest for future studies of carbon migration in a full carbon device in steady-state.
One potential method for in-situ analysis of material compositions is Laser-Induced Breakdown Spectroscopy (LIBS) [9] [6]. LIBS permits to distinguish between different hydrogen isotopes through the observation of isotopic shifts in the spectra emitted by the laser-induced plasma [7]. But the very small isotopic shift in emission from atomic carbon is more challenging to resolve due to the higher nuclear mass, as low light detection limit and the ability to observe multiple spectroscopic lines required for LIBS. A potential solution to this challenge is to observe the emission not from atomic carbon but from diatomic molecules containing carbon such as C_2, CO,

CH or CN, that are also present in the plasma [5] [1]. This method is called Laser Ablation Molecular Isotopic Spectroscopy (LAMIS) and the following analyses utilise the molecule C_2, which is present in a laser-induced plasma produced on a carbon surface without the need for impurities such as Oxygen, Nitrogen or Hydrogen.
LAMIS is essentially LIBS for molecules released during the ablation process, and therefore a valid option for such an in-situ technique. This text will show the suitability of LAMIS for the measurement of carbon isotope distributions on graphite PFCs with a post-mortem study. We will first describe the gas injection experiment and setup used for ex-situ analysis. Next, the method for analysing the spectra to obtain the ^{13}C content in the ablated volume is explained and discussed. Subsequently, a first study on individual PFCs from the TDU will be used to demonstrate the capabilities of LAMIS and the result will be compared to NRA measurements of ^{13}C depth and spatial resolution and finally compared to simulations with the ERO2.0 code. ERO2.0 is a Monte Carlo impurity transport and PWI code utilising a plasma background from plasma boundary solver EMC3-EIRENE.

2 Experimental

W7-X is a Helias-type stellarator with five-fold toroidal symmetry represented by 5 modules denoted with the index 1 to 5. Each module has a lower and an upper divertor unit each with multiple vertical and horizontal divertor modules containing multiple target elements (see fig. 1). The presented analyses were done on two target elements from the horizontal, lower divertor of modules 3 and 5. They are labelled as TE01 of HM39TM200h and TE07 of HM58TM200h.
Prior to extraction, $^{13}CH_4$ was injected into a hydrogen plasma through gas valves in the lower TDU of module 3 in the last plasma experiment of OP1.2b. The gas nozzles were situated between target elements TE04 and TE05 of divertor module HM39TM200h. About 4×10^{22} molecules were injected during a series of H plasmas in standard

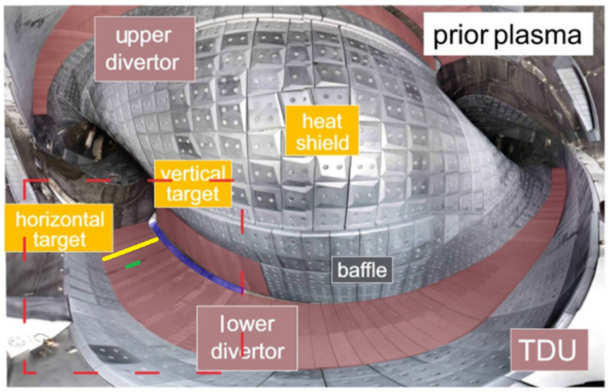

Figure 1: Picture of the TDU in W7-X before usage. In the marked area, location of injection (green), loaction of the nearest analysed TDU element (yellow) and the pumping gap (blue) are shown.

divertor configuration accumulating 330s of plasma duration [4]. Minimum distance between gas nozzles and the closest analysed divertor finger is 165 mm in toroidal direction. Further information about the experiment is given in [4].
Both elements have been extracted at the end of OP 1.2b from the W7-X vessel and cut along poloidal direction into smaller blocks (10 mm toroidal $\times$ 25 mm poloidal $\times$ 5 mm thick, sometimes smaller in poloidal direction depending on the structure of the surface) which fit into the sample holder of the NRA setup.

The setup used for the ex-situ study presented in this article consists of a laser system including optical elements for delaying laser pulses, the sample chamber with vacuum equipment and the spectrometer including optical elements for light collection (see fig. 2).
An EKSPLA PL2241CSH-TH Nd:YAG laser generates the 2nd ($\lambda = 532$ nm) and 3rd ($\lambda = 355$ nm) harmonic of the amplifier output ($\lambda = 1064$ nm) and provides laser pulses for the LIBS studies with each of the three wavelengths at different outputs. All three pulses are released at approximately the same time and have a pulse duration of $\tau = 35$ ps. In order to enhance the signal strength, double pulse scheme was used. The laser pulses with wavelengths $\lambda = 355$ nm

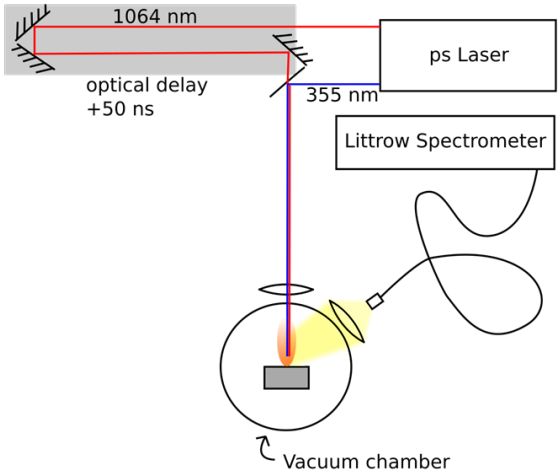

Figure 2: schematic of the LAMIS setup with laser system, vacuum chamber and spectrometer

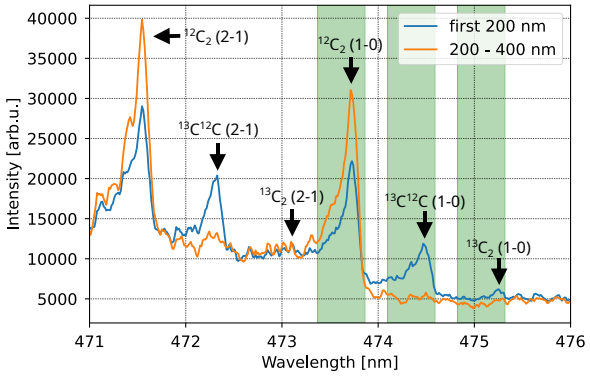

Figure 3: blue: spectrum taken from the first 200 nm of a TDU on a position with high ^{13}C content. The content calculated from this spectrum is 84%. orange: spectrum taken from the depth of 200 nm to 400 nm of a TDU on a position with reasonable ^{13}C content. The content calculated from this spectrum is 12%.

and $\lambda = 1064\,\mathrm{nm}$ have been used for the LAMIS measurement. The laser pulse with $\lambda = 355\,\mathrm{nm}$ is directly focussed ($f = 500\,\mathrm{mm}$) into the sample chamber and thus onto the material's surface. The second laser pulse with $\lambda = 1064\,\mathrm{nm}$ is first delayed optically by $\Delta t = 50\,\mathrm{ns}$ and then focussed into the plasma generated by the first laser pulse on the material surface. The angle between both beampaths on the surface is $\alpha = 5°$. The crater left behind after ablation by each pulse pair is ~700 µm in diameter and 200 nm in depth.

The experimental chamber is either at vacuum ($p = 1 \times 10^{-7}\,\mathrm{mbar}$) or at low pressure ($p = 1.5\,\mathrm{mbar}$) filled with nitrogen. Outside the chamber at an angle of $\beta = 5°$ to the beampath of the first laser pulse a concave aluminium mirror is used for collection of light, which is then led into a spectrometer by an optical fibre (d =1.5 mm, NA = 0.22). The spectrometer used for spectral analysis is a custom-built spectrometer in littrow arrangement optimized for high èndue (62 µm^2 sr). The spectrometer observes the wavelength interval 466 nm to 480 nm for an analysis of the 1-0 vibrational bands of the C_2 Swan bands ($d^3\Pi_g \rightarrow a^3\Pi_u$ transition).

3 Results

Figure 3 shows spectroscopic recordings of the C_2 Swan band from the position of highest ^{13}C content taken from the plasmas of the first and second laser pulses respectively. For further analysis, intensities were integrated over a spectroscopic span of 0.5 nm from the band head towards blue (integrated wavelength spans for $^{12}C_2$: 473.37 nm to 473.87 nm, for $^{13}C^{12}C$: 474.10 nm to 474.60 nm and for $^{13}C_2$: 474.83 nm to 475.33 nm). It is assumed that all three isotopologues have the same rovibrational population and emission behaviour. The relative intensities of the three bands carry information about isotopic composition of ablated material with good spatial resolution. If the relative integrated intensities are proportional to the relative abundances of the isotopologues, then the content of ^{13}C as fraction of total carbon in the ablated volume, represented by the sum of $^{13}C_2$, $^{12}C_2$ and $^{13}C^{12}C$, can be calculated by:

$$\frac{n_{^{13}C}}{n_C} = \frac{2 \cdot I_{^{13}C_2} + I_{^{13}C^{12}C}}{2 \cdot (I_{^{13}C_2} + I_{^{13}C^{12}C} + I_{^{12}C_2})}$$

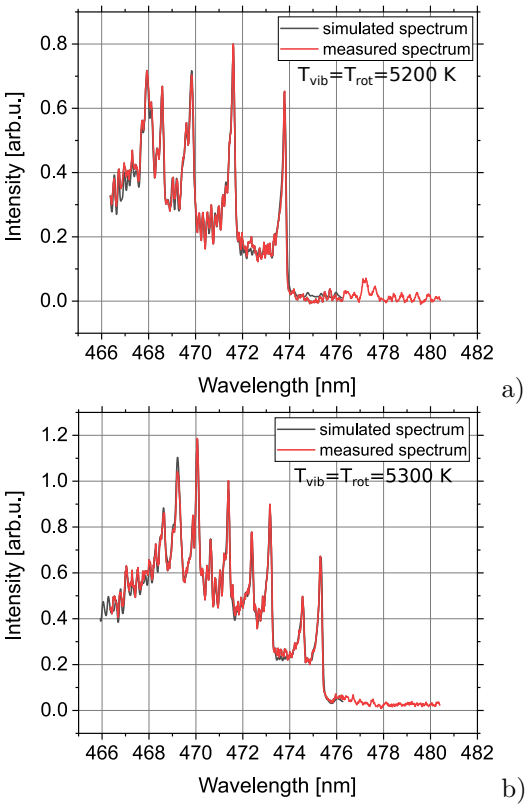

Figure 4: spectra from measurements and fitted simulated spectra for a) a case without ^{13}C and b) a case with maximum ^{13}C.

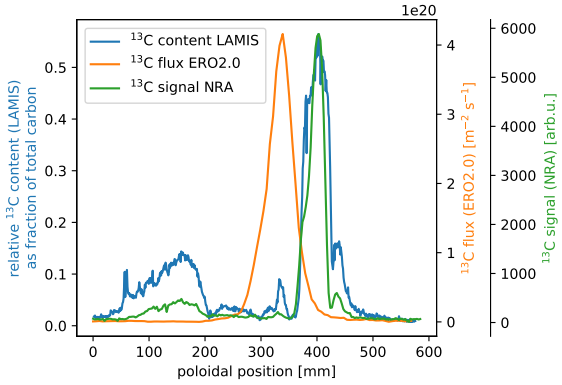

Figure 5: ^{13}C distribution on TE01 of HM39TM200h as measured by LAMIS, NRA and simulated by ERO2.0

Here I is the integrated intensity of the respective bands.
The spectra were fitted with simulated spectra using the program Pgopher, which provides emission spectra simulations of molecule mixtures [15]. The necessary molecular constants of the three C_2 isotopologues were extracted from the ExoMol database [14]. For this, rotational and vibrational temperatures are assumed to be equal and so were emission characteristics of all three isotopologues. In figure 4 two sample spectra and their fitted simulations are shown. Figure 4 a) shows measured and simulated spectra of a measurement where no ^{13}C was detected. The simulation finds a single rotation and vibrational (rovibrational) temperature of (5200 ± 21) K. The spectrum and fitted simulation with highest ^{13}C in this study is presented in figure 4 b). The rovibrational temperature found for this spectrum is (5300 ± 14) K. The given errors are an estimate of the fitting program and probably bigger due to the small fitted spectroscopic interval. These simulations can provide more information about the LAMIS plasma, but a more detailed analysis is going to be subject of future studies.

The analysed element closer to the injection location was target element TE01 of HM39TM200h. With a distance of minimal 165 mm, this element was located in the wake of the injection, but not in the

zone of strongest direct deposition after dissociation in the plasmas. The ^{13}C distribution as measured by LAMIS and NRA is shown in figure 5. The scale on the x-axis shows the poloidal location relative to the pumping gap (cf. fig. 1). The results of both analyses agree on the position and shape of ^{13}C deposition zones. Maxima in ^{13}C content around 400 mm poloidal coordinate on the target element are due to direct deposition after dissociation of $^{13}CH_4$ in the hot edge plasma of W7-X. A second deposition zone appears between 0 mm to 200 mm poloidal coordinate. No direct deposition from the gas injection is expected here, but ^{13}C can reach this area by dissociation and transport through the plasma including multiple erosion/deposition steps, thus migration. Note that the zone around 150 mm poloidal coordinate reflects the main horizontal strike-line, thus a net erosion zone in normal plasma conditions [4]. The causes of ^{13}C deposition in this normally erosion dominated zone have not yet been identified.
The ^{13}C flux onto the element as simulated by ERO2.0 is also shown in figure 5. The simulation this close to the injection location only takes direct ^{13}C deposition into account. For that reason, ^{13}C content caused by migrating ^{13}C is not predicted. Only the peak in ^{13}C content from direct deposition after injection appears between 270 mm to 410 mm poloidal coordinate. The maxima in simulated ^{13}C and in measured ^{13}C surface content are shifted in poloidal position by about 100 mm. This is probably due to neglection of E×B drift in the simulation or local changes in plasma parameters induced by the injection in its vicinity. Movement of the strike line due to toroidal currents in the plasma is another possible explanation. Further investigations will be done in a modelling focussed paper in the future.

Element TE07 of HM58TM200h was located significantly further away from the injection location, in a different Module, than TE01 of HM39TM200h. ^{13}C content as measured by LAMIS and ^{13}C flux onto the element as simulated by ERO2.0 are shown in figure 6. Here, maxima in simulation and measurement are in better agreement than on element TE01 of HM39TM200h, because all ^{13}C being deposited reaches TE07 of HM58TM200h through transport in accordance with background impurities. No direct deposition is expected this far from the injection location.

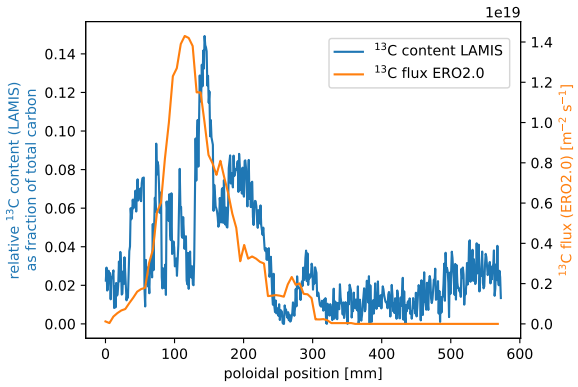

Figure 6: ^{13}C distribution on TE07 of HM58TM200h as measured by LAMIS and simulated by ERO2.0

4 Conclusion

The ex-situ performed NRA and LAMIS analyses of target element TE01 of TDU module HM39TM200h show generally good agreement on measured ^{13}C distribution. Both analyses were conducted along poloidal lines that were shifted toroidally by about 6 mm, which is expected to be small in relation to the changes in deposition behaviour in this region. The only deviation between the two measurements appears at the position of strong local deposition. Maximum ^{13}C content relative to ^{13}C content in deposition zone caused by migration is higher in NRA results than in LAMIS results. The causes of this deviation have not yet been resolved.
Relative to this, the local deposition zone as simulated by ERO 2.0 is shifted for about 100 mm towards the pumping gap. Multiple deposition/erosion steps were not yet taken into account in this simulation. The effort to take into account E×B drift and multiple erosion/deposition steps are ongoing. The observed shift in direct deposition might have been caused by neglection of E×B drift, changes in local plasma parameters induced by the injection or shift of the strike line due to toroidal currents in the plasma.

The deposition due to multiple erosion/deposition steps seen on TE07 of divertor module HM58TM200h shows more agreement between simulated and measured ^{13}C deposition. In case the shift of maximum ^{13}C deposition on divertor module HM39TM200h is due to toroidal currents in the plasma, no shift of ^{13}C deposition after multiple erosion/deposition steps is expected on TE07 of HM58TM200h. From the findings so far, we conclude that both, the method proposed for analysing carbon isotope content and the proposed way to analyse Swan bands to access ^{13}C content produce results that are in good agreement with an established way to measure ^{13}C content of PFCs. Although these findings do not demonstrate in-situ utilisation of this method, they do show that this method can determine ^{13}C isotopic content of graphite with high resolution ex-situ. Because LIBS has been utilised for in-situ material analysis [9] and the physics behind LIBS and LAMIS are similar, LAMIS in-situ implementation should be considered for future studies of erosion and deposition in stellarators with actively cooled divertor modules.

5 Acknowledgement

This work has been carried out within the framework of the EUROfusion Consortium, funded by the European Union via the Euratom Research and Training Programme (Grant Agreement No 101052200 — EUROfusion). Views and opinions expressed are however those of the author(s) only and do not necessarily reflect those of the European Union or the European Commission. Neither the European Union nor the European Commission can be held responsible for them.

References

[1] A. A. Bol'shakov, X. Mao, J. J. González, and R. E. Russo. Laser ablation molecular isotopic spectrometry (LAMIS): current state of the art. *Journal of Analytical Atomic Spectrometry*, 31(1):119–134, 2016.

[2] J. Boscary, A. Peacock, R. Stadler, B. Mendelevitch, H. Tittes, J. Tretter, M. Smirnow, and C. Li. Actively Water-Cooled Plasma Facing Components of the Wendelstein 7-X Stellarator. *Fusion Science and Technology*, 64(2):263–268, Aug. 2013.

[3] H.-S. Bosch, T. Andreeva, R. Brakel, T. Brauer, D. Hartmann, A. Holtz, T. Klinger, H. Laqua, M. Nagel, D. Naujoks, K. Risse, A. Spring, T. S. Pedersen, T. Rummel, P. van Eeten, A. Werner, and R. Wolf. Engineering Challenges in W7-X: Lessons Learned and Status for the Second Operation Phase. *IEEE Transactions on Plasma Science*, 46(5):1131–1140, May 2018.

[4] S. Brezinsek, C. P. Dhard, M. Jakubowski, R. König, S. Masuzaki, M. Mayer, D. Naujoks, J. Romazanov, K. Schmid, O. Schmitz, D. Zhao, M. Balden, R. Brakel, B. Butterschoen, T. Dittmar, P. Drews, F. Effenberg, S. Elgeti, O. Ford, E. Fortuna-Zalesna, G. Fuchert, Y. Gao, A. Goriaev, A. Hakola, T. Kremeyer, M. Krychowiak, Y. Liang, C. Linsmeier, R. Lunsford, G. Motojima, R. Neu, O. Neubauer, J. Oelmann, P. Petersson, M. Rasinski, M. Rubel, S. Sereda, G. Sergienko, T. S. Pedersen, T. Vuoriheimo, E. Wang, T. Wauters, V. Winters, M. Zhao, and R. Yi. Plasma-Surface Interaction in the stellarator W7-X: Conclusions drawn from operation with graphite Plasma-Facing Components. *Nuclear Fusion*, Nov. 2021.

[5] M. Dong, X. Mao, J. J. Gonzalez, J. Lu, and R. E. Russo. Carbon Isotope Separation and Molecular Formation in Laser-Induced Plasmas by Laser Ablation Molecular Isotopic Spectrometry. *Analytical Chemistry*, 85(5):2899–2906, Mar. 2013.

[6] M. Hubeny, D. Hoschen, O. Neubauer, R. Hoek, G. Czymek, D. Naujoks, D. Hathiramani, D. Bardawil, B. Unterberg, R. Konig, S. Brezinsek, C. Linsmeier, and X. Team. Progress on MATEO probe heads and observation system. *Fusion Engineering and Design*, page 5, 2021.

[7] C. Li, C.-L. Feng, H. Y. Oderji, G.-N. Luo, and H.-B. Ding. Review of LIBS application in nuclear fusion technology. *Frontiers of Physics*, 11(6):114214, Dec. 2016.

[8] J. Likonen, E. Alves, A. Baron-Wiechec, S. Brezinsek, J. P. Coad, A. Hakola, K. Heinola, S. Koivuranta, G. F. Matthews, P. Petersson, M. Rubel, C. Stan-Sion, A. Widdowson, and JET-EFDA Contributors. First results and surface analysis strategy for plasma-facing components after JET operation with the ITER-like wall. *Physica Scripta*, T159:014016, Apr. 2014.

[9] G. Maddaluno, S. Almaviva, L. Caneve, F. Colao, V. Lazic, L. Laguardia, P. Gasior, and M. Kubkowska. Detection by LIBS of the deuterium retained in the FTU toroidal limiter. *Nuclear Materials and Energy*, 18:208–211, Jan. 2019.

[10] M. Mayer, M. Balden, S. Brezinsek, V. V. Burwitz, C. P. Dhard, A. Dudek, G. Ehrke, Y. Gao, H. Greuner, R. Guimarães, P. Hiret, S. Klose, R. König, M. Krause, R. Laube, M. Laux, D. Naujoks, R. Neu, J. Oelmann, C. Ruset, T. S. Silva, R. Yi, D. Zhao, and W7-X Team. Material erosion and deposition on the divertor of W7-X. *Physica Scripta*, T171:014035, Jan. 2020.

[11] M. Mayer, S. Krat, A. Baron-Wiechec, Y. Gasparyan, K. Heinola, S. Koivuranta, J. Likonen, C. Ruset, G. de Saint-Aubin, A. Widdowson, and JET Contributors. Erosion and deposition in the JET divertor during the second ITER-like wall campaign. *Physica Scripta*, T170:014058, Dec. 2017.

[12] R. A. Pitts, J. P. Coad, D. P. Coster, G. Federici, W. Fundamenski, J. Horacek, K. Krieger, A. Kukushkin, J. Likonen, G. F. Matthews, M. Rubel, J. D. Strachan, and J.-E. contributors. Material erosion and migration in tokamaks. *Plasma Physics and Controlled Fusion*, 47(12B):B303–B322, Dec. 2005.

[13] J. Romazanov, D. Borodin, A. Kirschner, S. Brezinsek, S. Silburn, A. Huber, V. Huber, H. Bufferand, M. Firdaouss, D. Brömmel, B. Steinbusch, P. Gibbon, A. Lasa, I. Borodkina, A. Eksaeva, C. Linsmeier, and JET Contributors. First ERO2.0 modeling of Be erosion and non-local transport in JET ITER-like wall. *Physica Scripta*, T170:014018, Dec. 2017.

[14] J. Tennyson, S. N. Yurchenko, A. F. Al-Refaie, E. J. Barton, K. L. Chubb, P. A. Coles, S. Diamantopoulou, M. N. Gorman, C. Hill, A. Z. Lam, L. Lodi, L. K. McKemmish, Y. Na, A. Owens, O. L. Polyansky, C. Sousa-Silva, D. S. Underwood, A. Yachmenev, and E. Zak. The ExoMol database: molecular line lists for exoplanet and other hot atmospheres. *Journal of Molecular Spectroscopy*, 327:73–94, Sept. 2016. arXiv: 1603.05890.

[15] C. M. Western. PGOPHER: A program for simulating rotational, vibrational and electronic spectra. *Journal of Quantitative Spectroscopy and Radiative Transfer*, 186:221–242, 2017.